A stimulated Raman loss spectrometer for metrological studies of quadrupole lines of hydrogen isotopologues
Lamperti, M., Rutkowski, L., Gatti, D., Gotti, R., Moretti, L., Polli, D.,Cerullo G. Marangoni, M.
Molecular Physics

DOI: https://doi.org/10.1080/00268976.2023.2196353
Link:
https://www.tandfonline.com/doi/citedby/10.1080/00268976.2023.2196353?scroll=top&needAccess=true

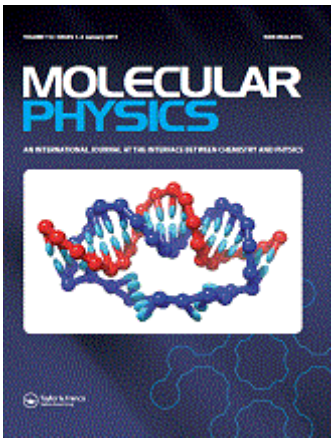

A Stimulated Raman Loss spectrometer for metrological studies of quadrupole lines of hydrogen isotopologues

Journal:	*Molecular Physics*
Manuscript ID	Draft
Manuscript Type:	Special Issue Paper
Date Submitted by the Author:	n/a
Complete List of Authors:	Lamperti, Marco; Insubria University - Como Campus, Dipartimento di Scienza e Alta Tecnologia Rutkowski, Lucile; Institut de Physique de Rennes; Rennes 1 University Gatti, Davide; Politecnico di Milano, Department of Physics; IFN CNR Gotti, Riccardo; Università degli Studi di Pavia, Dipartimento di Ingegneria Industriale e dell'Informazione Moretti, Luca; Politecnico di Milano, Department of Physics; IFN CNR Polli, Dario; Politecnico di Milano, Department of Physics; IFN CNR Cerullo, Giulio; Politecnico di Milano, Department of Physics; IFN CNR Marangoni, Marco; Politecnico di Milano, Department of Physics; IFN CNR
Keywords:	Raman spectroscopy, high-resolution spectroscopy, hydrogen spectroscopy

H_2 and its isotopologues are benchmark systems to test QED and constrain physics beyond the standard model, thanks to highly accurate theoretical determination of their energy levels. Lacking a dipole moment, H_2 is difficult to investigate experimentally, with state-of-art measurements on rovibrational transitions lagging theory by about one order of magnitude in uncertainty. We have developed and a comb-calibrated spectrometer based on stimulated Raman scattering, and applied it to surpass the best current theoretical determination of the fundamental Q(1) transition, paving the way for ultraprecise determination of fundamental rovibrational energies in molecular hydrogen. In this paper we discuss in detail the rationale of the spectrometer and the necessary steps needed to bring a stimulated Raman spectrometer to sub-MHz accuracy.

A Stimulated Raman Loss spectrometer for metrological studies of quadrupole lines of hydrogen isotopologues

M. Lamperti[1,*] ORCID 0000-0001-5972-8723, L. Rutkowski[2] ORCID 0000-0002-9804-0136, D. Gatti[1] ORCID 0000-0001-9335-821X, R. Gotti[1,†] ORCID 0000-0003-3691-814X, L. Moretti[1] ORCID 0000-0001-8092-0752, D. Polli[1] ORCID 0000-0002-6960-5708, G. Cerullo[1] ORCID 0000-0002-9534-2702, M. Marangoni[1] ORCID 0000-0002-0522-149X

[1] *Dipartimento di Fisica - Politecnico di Milano and IFN-CNR, Via Gaetano Previati 1/C, 23900 Lecco, Italy*

[2] *Univ Rennes, CNRS, IPR (Institut de Physique de Rennes)-UMR 6251, F-35000 Rennes, France*

* *marco.lamperti@uninsubria.it, currently at Dipartimento di Scienza e Alta Tecnologia – Università degli studi dell'Insubria, via Valleggio 11, 22100 Como, Italy*

[†]*Currently at Dipartimento di Ingegneria Industriale e dell'Informazione, Università di Pavia, Via Ferrata 5, 27100 Pavia, Italy*

We discuss layout and performance of a high-resolution Stimulated Raman Loss spectrometer that has been newly developed for accurate studies of spectral lineshapes and line centre frequencies of hydrogen isotopologues and in general of Raman active transitions. Thanks to the frequency comb calibration of the detuning between pump and Stokes lasers and to an active alignment of the two beams, the frequency accuracy is at a level of 50 kHz. Over the vertical axis the spectrometer benefits from shot-noise limited detection, signal enhancement via multipass cell, active flattening of the spectral baseline and measurement times of few seconds over spectral spans larger than 10 GHz. Under these conditions an efficient averaging of Raman spectra is possible over long measurement times with minimal distortion of spectral lineshapes. By changing the pump laser, transitions can be covered in a very broad frequency span, from 50 to 5000 cm^{-1}, including both vibrational and rotational bands. The spectrometer has been developed for studies of fundamental and collisional physics of hydrogen isotopologues and has been recently applied to the metrology of the Q(1) 1-0 line of H_2.

Keywords: Raman spectroscopy; high-resolution spectroscopy; hydrogen spectroscopy.

1. Introduction

Over almost three decades, from the 70s to the 90s, Coherent Raman Scattering[1] (CRS) spectroscopy has been the approach of election for intensive spectroscopic studies of molecular hydrogen and its isotopologues, namely D_2 and HD. Several reasons underpinned these studies. The large Raman cross section[2] of molecular hydrogen and its sparse Raman spectrum made it among the best gas candidates for the realization of Stimulated Raman amplifiers to shift the wavelength of pulsed lasers[3], [4]. In combustion[5] and plasma[6] diagnostic, H_2 was introduced as a probe for temperature determinations via Coherent Anti-Stokes Raman Scattering[1] (CARS), thanks to its largely separated Raman lines and to the chance to extract the temperature from their relative intensities. As the determination of intensities implied the knowledge of Raman lineshapes, calculations were carried out on the effects of collisions on the vibrational spectra[7] of H_2 and its main isotopologues. The calculated spectra were comparatively analysed against experimental data mostly acquired by Stimulated Raman Scattering[1] (SRS), which offers the advantage not to distort spectral lineshapes[8] with respect to CARS. Collisional pressure shift and broadening coefficients[9]–[13] and their temperature dependencies[14]–[16] were measured for all major isotopologues and also related to the angular and radial dependence of the molecular interaction potential[17]. To discriminate among different line-broadening mechanisms, such as those arising from elastic and inelastic collisions, CRS measurements were performed on both rotational[18], [19] and vibrational bands, because of their different collisional physics, as well as on depolarized[20], [21] (or anisotropic) and polarized (isotropic) components of Q transitions. On another front, the amenability of H_2 to quantum calculations of its energy levels[22] led to the first comparisons between experimental and calculated energies and to the development of more and more refined lineshape models to extrapolate zero-pressure line centres from collision-perturbed lineshapes[23]. The turn of the millennium happened to be an inflection point for H_2 studies, whose interest progressively declined together with the use of Coherent Raman spectrometers.

A resurgence of interest for H_2 rovibrational spectroscopy was triggered in 2011 by an accurate list of transition frequencies obtained by Komasa and Pachucki[24] from ab-initio quantum-electrodynamic calculations. The importance of comparing this database with accurate laboratory measurements was early recognized by the group of Wim Ubachs, who had shown in 2008 [25] the potential for fundamental physics of Lyman and Werner bands of H_2, as a testbed for new physics, such as fifth forces[26], extra-dimensions[27] and physics beyond the Standard Model[28]**Error! Reference source not found.**. In 2019, a new refined line list appeared with relativistic corrections up to $\alpha^5 m$ bringing the accuracy of theoretical calculations to the sub-MHz level, which is the current benchmark[29]**Error! Reference source not found.**. The effect of these papers was to revitalize experimental investigations. These could benefit from the unprecedented advantage of an absolute frequency scale given by the newly invented frequency combs. A first milestone was obtained by Resonantly-Enhanced Multi-Photon Ionization[30] (REMPI): in this approach vibrationally excited molecules are selectively ionized through resonance multi-photon absorption of a pulsed ultraviolet laser and then selectively detected from the mass of the generated ion. The combination of comb calibrated laser frequencies and of a molecular beam suppressing collisional and Doppler broadening enabled the Q(J) transition frequencies of the fundamental vibrational band of H_2, D_2 and HD to be measured with an 8 MHz accuracy, almost an order of magnitude better than previous measurements performed by Fourier Transform Spectroscopy[31] and CRS[10]**Error! Reference source not found.**. Recently, this benchmark for REMPI was substantially improved for the S(0) fundamental rovibrational line of D_2, down to 17 kHz[32], thanks to a more efficient vibrational excitation of the molecules and to a better control of Type B errors induced by the fine structure of the molecule.

In parallel, taking advantage of the enormous progress in the quality of mirrors, modulators and lasers in the telecom spectral range, a number of cavity-enhanced absorption spectrometers (CEAS) were developed to address the overtone lines of H_2 and its isotopologues in a Doppler broadening regime. The very small absorption cross-section of their quadrupole transitions is compensated in CEAS by a strongly increased effective absorption path length[33]. The first measurements

calibrated against a simple wavemeter were successfully compared with the first theoretical line list within 20 MHz[34]–[36]. The addition of comb calibration resulted in uncertainty budgets below 1 MHz for several quadrupole lines[37]–[42], primarily of D_2 whose 2-0 band falls in the highly accessible telecom range. The CEAS benchmark is on the S(2) line of D_2, with an uncertainty of about 170 kHz[42]. In cavity measurements the lineshape model adopted for the fitting of experimental spectra was soon recognized as a limiting factor for the uncertainty budget, due to the nontrivial impact of velocity changing collisions and speed-dependent effects in a colliding environment of H_2 molecules[43]. The experimental progress in the sensitivity of CEAS setups has been thus accompanied by a strong effort to improve the accuracy of lineshape models, with the testing of speed-dependent billiard ball profiles[44], the implementation of a β-corrected[45] Hartmann Tran Profile (βHTP)[46], the integration in βHTP of collisional parameters obtained through *ab initio* calculations: this enables to reduce the number of fitting parameters[47] and to assign physically meaningful values to collisional parameters showing strong correlation in the fitting. Another benefit of fixing some collisional parameters is to retrieve meaningful confidence intervals for the parameters fitted[48] **Error! Reference source not found.**. On another closely related front, namely the heteronuclear HD isotopologue that exhibits weak dipole-allowed transitions, several measurements recently attained final accuracies in the 10-150 kHz range: this happened for the fundamental R(0) line studied by REMPI on a molecular beam[49], for the R(1) 2-0 line investigated at different pressures and temperatures by both sub-Doppler[50], [51] and Doppler broadening spectroscopy[52], [53], for the recently addressed R(1), R(3), P(3)[54], R(0)[52] 2-0 lines, the latter observed at cryogenic temperatures and Pascal-level pressures in an optical cavity. For the largely studied R(1) 2-0 line, the agreement within 200 kHz of 4 completely different determinations is highly significant, also considering the difficulty to fit and interpret the dispersive lineshape of Lamb dips unexpectedly encountered in sub-Doppler measurements[55]–[57].

In the past decade, apart from REMPI measurements, fundamental quadrupole transitions have almost never been addressed experimentally, mainly due to the difficulty to achieve high-sensitivity

CEAS in the mid-infrared, where the quality of lasers, mirrors, modulators and detectors is poorer, and the costs are higher. The CRS approach was chosen for the metrology of Tritium-bearing molecules[58]**Error! Reference source not found.** (T_2, DT, HT) and the experimental validation of calculated broadening and shift coefficients for rotational lines of D_2[48]**Error! Reference source not found.** and HD[59]. However, in both cases the setups were reminiscent of those developed before year 2000 for Raman spectroscopy over large temperature scales[15], [60], as based on nanosecond lasers that limit resolution and accuracy to 50 and 6 MHz[58], respectively. For CRS studies at higher resolution, the traditional approach firstly proposed by Owyung[61]**Error! Reference source not found.** and later improved by Rosasco[9], [62] and Forsman[63] was based on a single longitudinal mode Ar-ion laser for the pump (488.0 nm, 300 mW, 15 MHz FWHM bandwidth for a 1 s average) and on a single-mode tuneable dye laser for the Stokes (592-593 nm, 200 mW, 1 MHz FWHM bandwidth for a 1 s average). The Raman signal was measured as stimulated Raman gain, which implies pump intensity modulation and synchronous detection of the Stokes intensity change. In the latest version of the spectrometer, Forsman et al.[63] managed to achieve a spectral resolution of 1 MHz by stabilization of the Ar laser to an external cavity, a frequency accuracy of 2 MHz by calibration of pump and Stokes frequencies against a pressure-tight temperature-stabilized off-axis Fabry Perot interferometer, and a signal-to-noise ratio (SNR) of 1000 in 1 s for the Q-branch of D_2 at a few amagat.

Our group, attracted by the versatility of SRS to address both vibrational and rotational transitions with well assessed near-infrared technology and by the chance to calibrate pump and Stokes laser frequencies against a frequency comb for maximum resolution and accuracy, discerned the potential to revisit and improve those layouts and develop a metrology-grade SRS spectrometer for quadrupole lines of homonuclear species and in general of Raman active lines. We have recently applied it to determine the transition frequency of the historically famous Q(1) line of the 1-0 band of H_2 at ≈ 4155 cm^{-1} with a combined uncertainty of $1.0 \cdot 10^{-5}$ cm^{-1} (310 kHz [64]), improving by 20 times the experimental benchmark[30] and by a factor of 2 the theoretical benchmark[29]. This

result comes from a frequency accuracy improved by a factor of 40 (50 kHz against 2 MHz) and by a signal-to-noise ratio increased by a factor of 8 as compared to Forsman et al.[63]**Error! Reference source not found.**. This paper provides a detailed description of the spectrometer and of its performance, by sequentially analysing all major parts of the apparatus, namely excitation and calibration laser sources, optical beamlines, gas chamber, comb referencing of pump and Stokes lasers, detection chain, procedures for acquisition, averaging and calibration of SRS spectra.

2. Setup

General layout

The spectrometer relies on an SRS process driven by two narrow-linewidth CW lasers whose frequency is calibrated against an optical frequency comb. The comb provides repeatability and absolute calibration of the detuning between pump and Stokes frequencies. The signal-to-noise ratio (SNR) is maximized by use of a multipass cell that enhances the interaction length between gas and laser fields and by implementing a detection chain that works at the shot noise limit: this limit is obtained by modulating at high frequency (several megahertz) the intensity of the Stokes laser and by performing lock-in detection of the stimulated Raman loss (SRL) imparted on the pump beam. Contributions to systematic errors from variations of thermodynamic parameters of the sample are minimized by active stabilization of both temperature and pressure of the gas, while spectral distortions induced by power changes of the Stokes laser while it is scanned across the Raman transition are quenched by an active stabilization of the Stokes power. Finally, as misalignment between pump and Stokes lasers was found to be responsible for systematic shifts of the measured line centre frequency, we introduced a system for active stabilization of the overlap between pump and Stokes beams in the multipass cell. The layout of the spectrometer is depicted in Fig. 1. It is composed of several parts discussed in detail in the following, namely laser sources, optical beam

lines, multipass cell, comb referencing, detection chain, SRL spectra acquisition, spectra averaging and calibration and active beam alignment.

Laser sources

The spectrometer makes use of three lasers sources, namely: i) an external-cavity (EC) diode laser (Toptica DL pro) as a pump beam of the SRS process, with tunability from 710 to 740 nm and power up to 40 mW; ii) an amplified distributed-feedback (DFB) Ytterbium fibre laser at 1064 nm (Koheras Boostik HP) as Stokes beam, featuring single-mode operation, piezo-electric frequency tuning over 15 GHz and optical power up to 15 W; iii) an Erbium:fiber mode-locked oscillator at 100 MHz (Menlo C-Fiber) followed by a home-made optical amplifier and supercontinuum stage for frequency comb calibration of pump and Stokes laser frequencies. This laser configuration is favourable to operate the spectrometer in the so-called inverse-Raman scattering regime, in which an intense Stokes laser is modulated and the SRL signal on the pump beam is detected. The choice of an EC diode laser for the pump beam brings several advantages: i) a high SNR on the measured SRL, thanks to a shot-noise-limited intensity spectrum (see section "Detection chain") and to the high quantum efficiency of silicon detectors around 700 nm; ii) the coverage of several Raman transitions, specifically all fundamental lines of the Q branch of H_2 around 4155 cm^{-1} (739 nm) and the S(0) line at 4497 cm^{-1} (720 nm), thanks to the broad wavelength tuning range; iii) a robust frequency locking to the comb thanks to the large dynamic range (few gigahertz) and high-bandwidth (kHz level) of the piezo-actuated frequency tuning port. During the spectral measurements, we keep the pump locked to the nearest comb tooth and exploit the piezo-modulation port of the Stokes laser to modify the detuning between the two cw lasers. This can be done over a 15 GHz range that fully covers Raman spectra at both low and high pressures.

Optical beamlines

The pump beamline starts with a single-mode optical fibre to spatially filter the beam and remove the laser astigmatism. The beam circularity is crucial to match it to the nearly confocal multipass

cell used as a gas chamber and to the co-propagating Stokes beam. At the fibre output the collimated pump beam passes through a telescope that shapes the beam to an optimized beam-waist radius of 220 μm in the middle of the cell. A fraction of the pump beam is split out from the initial fibre patch and sent to the comb calibration part of the setup. The Stokes laser does not require any spatial filtering because of the intrinsically high spatial quality guaranteed by the fibre format. A beam sampler splits a small fraction of it towards the comb calibration unit, while the major fraction sequentially crosses an acousto-optic modulator for power stabilization, an electro-optic intensity modulator (R7v-10R3-YAG from Qubig) used for the synchronous detection of the SRL signal, and a telescope to optimize the injection into the multipass cell (with a beam waist of 265 μm at its centre). Reflecting optics are used for all telescopes to quench parasitic etaloning effects that might alter the flatness of the spectral baseline. Stokes and pump beams are recombined before the cell by a dichroic mirror and brought to the same linear polarization state by a Glan-Thompson polarizer to avoid any distortion of the SRL response[Error! Reference source not found.]. At the cell output a prism extracts the pump beam and redirects it to an amplified home-built silicon photodiode for SRL detection. A notch filter at 1064 nm protects the photodiode from the Stokes stray light, avoiding any undesired signal background.

Gas chamber

The gas chamber consists of a multipass cell with a geometrical length of 42 cm that provides, after 70 bounces, an effective interaction length $L = 30$ m. This enhances the SRL signal since the SRS processes is phase matched along the whole interaction length[Error! Reference source not found.]. The nearly confocal Herriott cell configuration sets for the recirculating beam injected under optimal conditions a spot radius changing from a minimum value $w_0 = \sqrt{\lambda L/2\pi}$ at the cell center to $\sqrt{2}w_0$ at the cell mirrors[65][Error! Reference source not found.]. The cell can contain gas in a pressure range from 10^{-3} to 5 bar and is equipped with broadband dielectric mirrors that guarantee a total transmission around 50% from 700 to 1100 nm. In typical conditions the injected Stokes power is 3 W while the

pump power at the SRL detector, which is relevant to compute the shot noise, is 350 μW. Pressure and temperature of the gas inside the cell are actively stabilized to ensure stable thermodynamic conditions and to allow an efficient averaging of multiple spectra acquired over long measurement times. A temperature uniformity better than 100 mK results from the thermal conductivity of the steel that the cell is made of, combined with a surrounding box made with thick Styrofoam and equipped with internal air circulation by two fans. The temperature is measured by a calibrated Pt100 probe and a 6 ½ digit multimeter with an overall accuracy of 50 mK. A LabView-based PID servo maintains a temperature stability < 30 mK by regulating the current passing through stripe heaters glued onto the cell. To maintain a constant pressure during the measurements and compensate for small leaks of the cell, a constant flow of about 10^{-2} L/min is established in the cell using two flow controllers, one at the gas inlet and another one at the cell output upstream the vacuum pump. The pressure inside the cell is measured via a calibrated pressure sensor with relative uncertainty better than 10^{-3}. Through a software PID control loop, the output flow is regulated to maintain a constant pressure inside the cell within 0.1 mbar.

Comb referencing

The comb referencing of pump and Stokes lasers is obtained by generating their respective beat notes (BNs) with frequency-doubled spectral portions of an octave-spanning comb supercontinuum (see Fig. 2): specifically, the Stokes laser is made to beat with the second harmonic of the 2128 nm part of the continuum while the pump laser with the second harmonic of the 1480 nm part of the continuum. Second harmonic generation (SHG) takes place in a periodically-poled lithium niobate crystal and in a periodically-poled lithium tantalate optical waveguide for Stokes and pump, respectively: the waveguiding medium is used because of its larger conversion efficiency to compensate for the small power spectral density of the comb around 1480 nm. This referencing scheme requires neither the knowledge nor the stabilization of the carrier-envelope frequency (f_{ceo}) of the comb to achieve an absolute measurement of the frequency detuning between pump and

Stokes lasers: this is because (see section "Spectra calibration and averaging") their beat-note signals are affected by the same $2f_{ceo}$ term arising from SHG, which cancels out in the subtraction of the two frequencies. The repetition frequency f_{rep} is thus the only comb parameter stabilized, against a GPS-disciplined Rb oscillator that acts as a master clock to calibrate also the beat notes. The stability of this clock is at a level 10^{-11} at 1 s, thus far in excess of the 10^{-9} frequency uncertainty limit of the spectrometer set by the beam pointing instability of the lasers (see section "Active alignment of the laser beams"). The instrumental broadening of the spectrometer is almost negligible thanks a short-term linewidth < 100 kHz for both pump and Stokes lasers. The spectral resolution of the SRS spectrometer exceeds by a factor of 10 that of the best previous realizations based on Argon and dye lasers.

Detection chain

The SRL signal corresponds to a Stokes-induced intensity change of the pump beam. In our experimental conditions it remains smaller than 10^{-3}, even at high pressure on the intense fundamental Q(1) line of H_2. To measure it at high signal-to-noise ratio (SNR) we recurred, as it is typical in any SRS measurement, to a synchronous detection approach in which the Stokes laser beam is intensity modulated at high frequency (9.7 MHz, in our case) and a lock-in amplifier (LI) extracts the amplitude of the modulation signal transferred to the pump beam. We evaluated the SNR of the detection chain by exploiting a built-in functionality of the adopted lock-in amplifier (H2FLI from Zurich Instruments) to measure, in a 1 Hz bandwidth, the relative intensity noise spectrum of the pump laser on the SRL photodiode, with no Stokes irradiation on the sample and thus no Raman loss. Figure 3a shows this spectrum as the ratio between the average root-mean-squared noise voltage measured by the lock-in amplifier and the DC voltage at the detector, thus in units that can be directly compared to the SRL. Three out of the five spectra shown in the figure are experimental and refer to the lock-in noise background (blue line), the lock-in plus detector noise background (i.e. with pump off, red line), and the noise under pump irradiation (yellow line), thus

with the addition of laser intensity and shot noise. While the noise from the lock-in is negligible, the noise from the detector is slightly smaller than the theoretical shot noise floor of $4.1 \cdot 10^{-8}$ $Hz^{-0.5}$ (purple line) calculated for a pump optical power of 350 μW, which we use in the experiments. Very importantly, at the Fourier frequency of 9.7 MHz used in our experiments, the intensity noise of the EC laser is above the shot noise level by only a factor of 1.1, indicating a very modest impact from the laser intensity noise. This can be better appreciated by calculating the quadrature sum of detector noise plus theoretical shot noise floor (green line), which closely approaches the total noise measured (at 9.7 MHz). We can thus conclude that the laser is shot noise-limited at high Fourier frequencies and that the detection chain works close to the quantum limit. An even higher sensitivity could be obtained with a less noisy detector and/or by increasing the pump laser power to reduce the shot noise floor (with an inverse square root behaviour). If we compare the total noise measured of $6.1 \cdot 10^{-8}$ $Hz^{-0.5}$ with the measured rms SRL signal peak of $7.6 \cdot 10^{-4}$, which holds for the Q(1) of H_2 at a pressure of 1 atm, we obtain a highly favourable SNR of 8000 on a single spectral point over a 1 s measurement time (approximately corresponding to the 1 Hz bandwidth). This is by factor of 8 better than any previous SRS spectrometer. Figure 3b reports typical spectra acquired at different pressures on the Q(1) fundamental rovibrational line of H_2. The measurement time varies from a minimum of 5 min at high pressure to a maximum of 1 h at low pressure. The figure legend reports the SNR of the measured spectra when the spacing between spectral points is 1 MHz: even at lower pressures, where the SNR is reduced by the lower gas density and the larger profile (dominated by Doppler broadening rather than by Dicke narrowing), the SNR is consistent with a statistical uncertainty on the line centre lower than 0.5 MHz, thus suitable for optical metrology.

Spectra acquisition

Spectral measurements are preceded by a coarse adjustment of the pump wavelength by means of an optical spectrum analyser to match the pump-Stokes frequency detuning to the target vibrational frequency. The pump laser frequency is then offset-locked to the nearest comb mode, 10 MHz

apart. The spectra are acquired by measuring the SRL signal with a 1 μs lock-in integration time while scanning the Stokes frequency over about 12 GHz around the centre of the transition. Depending on the gas pressure and thus on the magnitude of the SRL signal, the frequency scans are repeated at rates of 0.1 Hz or 1 Hz, corresponding to frequency tuning speeds of ~2.4 and ~24 kHz/μs, respectively. The scan rate and the LI integration time are such that no appreciable spectral distortion is introduced by the low-pass filter of the LI. For the calibration of the frequency axis the comb-Stokes beat note is synchronously digitized with the SRL signal at a fast rate using a 100 MSa s^{-1} 14 bit National Instrument PXIe-7961 board. Its onboard FPGA processor (NI-5781) allows the beat note frequency to be calculated in real time every 10 μs by Fast Fourier Transform processing of data segments composed of 1024 samples. This is equivalent to having SRL points spectrally separated by 24 or 240 kHz depending on the adopted scan rate. The absolute frequency is reconstructed in post-processing by unwrapping the measured beat note frequency with the procedure described in detail in the next section. The total acquisition time of an SRL spectrum for a given line and under given thermodynamic conditions varies from 5 to 30 min depending on the pressure. Longer times can be implemented to further enhance the SNR thanks to the robustness of the comb calibrated frequency measurement.

It is worth emphasizing that without a proper power stabilization of both pump and Stokes lasers the shot-noise limit above discussed is far from being the ultimate limitation to the quality of an SRL spectrum. Spectral distortions may easily occur because in an SRS process the measured pump intensity change is linearly proportional to pump and Stokes powers that can fluctuate appreciably over time during spectral acquisitions (even if these are performed at a fast rate). Apart from the normal power drift of any laser, Stokes power fluctuations occur due to the piezo-actuated frequency scans, as further enhanced by etalon-induced fringes. Figure 4 quantifies this issue by reporting the time-dependent power of the Stokes laser when its frequency is kept fixed (panel a, blue trace), when it is varied at 1 Hz in a typical scan (panel b, blue trace), and when a proper active power stabilization is switched on (red trace in both panels): the fluctuations are of the order of 10^{-2}

without stabilization and 10^{-4} with active stabilization. The power stabilization is thus mandatory to preserve the shot-noise limit in SRL spectra and to keep distortions of the spectral lineshape below the noise level. It is implemented via an acousto-optic modulator whose diffraction efficiency is controlled by a PID servo to stabilize the power of the 0th diffraction order on a monitoring detector.

Spectra calibration and averaging

The absolute calibration of spectra is performed by assigning to each spectral point the corresponding value of the Raman detuning $\Delta\nu = \nu_p - \nu_s = n_p f_{\mathrm{rep}} \pm f_{\mathrm{bn,p}} + 2f_{ceo} - (n_s f_{\mathrm{rep}} \pm f_{\mathrm{bn,s}} + 2f_{ceo})$, where ν_p and ν_s are the optical frequencies of pump and Stokes lasers, respectively, which can be written as an integer number times the comb repetition frequency ($n_x f_{rep}$) plus or minus the beat note $f_{bn,x}$ between the laser and the frequency comb. The frequency detuning can be expressed in compact form as $\Omega = \Delta n\, f_{\mathrm{rep}} \pm f_{\mathrm{bn,p}} \pm f_{\mathrm{bn,s}}$, where $\Delta n = n_p - n_s$. The sign of $f_{bn,s}$ is given by the direction of the scan, the sign of $f_{bn,p}$ is determined by the sign of the lock, and Δn can be determined minimizing the discrepancy between the measured and theoretical transition frequency, which is known with an uncertainty much lower than f_{rep}.

The acquisition board acquires synchronously the SRL signal ad the value of $f_{bn,s}$ in the range $0 \div f_{rep}/2$, which corresponds to 50 MHz in our case. The result is a beat note frequency which follows a sawtooth pattern as shown in Fig. 5a. The measured $f_{\mathrm{bn,s}}$ is then unwrapped to retrieve a monotonically increasing frequency, representing the relative frequency of the Stokes laser with respect to a comb tooth (Fig. 5b). When $f_{\mathrm{bn,s}}$ is close to DC or to $f_{\mathrm{rep}}/2$, the beat note power is too low for a correct determination of its frequency, due to AC coupling and low-pass filtering below 50 MHz to avoid aliasing. To compute the beat-note in these blank regions we perform a quadratic interpolation of $f_{\mathrm{bn,s}}$ in an interval of 50 MHz around the blank region. From the standard deviation of the residuals of these repeated quadratic fits used for the interpolations of $f_{\mathrm{bn,s}}$ over time we determine a precision of 80 kHz for the frequency calibration of each single spectral point.

Once single spectra are calibrated in frequency, they can be combined to produce an average spectrum. As their points are not acquired on a regular, evenly spaced frequency grid, we perform a binning of spectral points by dividing the frequency axis in 1 MHz wide bins and by averaging all the points falling inside the same bin.

Active alignment of the laser beams

We experimentally found that a small angular tilt between pump and Stokes beams translated into a shift of their actual frequency detuning. In our setup, manual alignment could guarantee an accuracy up to 300 μrad, which corresponds to frequency fluctuations of more than 1 MHz on repeated measurements.

To reduce this source of uncertainty, we implemented an active alignment of the Stokes beam onto the pump. The system is illustrated in Fig. 6a: the superimposed pump and Stokes beams are sampled right after the dichroic beam combiner, then further split into two replicas impinging onto different regions of a CMOS colour camera. The first replica passes through a lens that images the plane of the beam combiner onto the sensor, while the second replica is made to propagate a total distance equal to that between the beam combiner and the centre of the cell before hitting the camera. We may refer to these planes as the near and far field (NF and FF, respectively).

The RGB colour filters of the camera sensor have different responses to the wavelengths of the pump and Stokes beams: the pump is maximally transmitted through the red channel, while the Stokes is equally transmitted through all channels. We can model the camera detection of the two beams through a matrix that maps the local intensity of the pump and Stokes beams, I_p and I_S, respectively, onto the RGB signals of the corresponding pixel:

$$\begin{pmatrix} R \\ G \\ B \end{pmatrix} = M \begin{pmatrix} I_p \\ I_S \\ 0 \end{pmatrix}.$$

The matrix M can be determined column by column by sending one beam at a time on the camera sensor and measuring the response of each colour channel. The above equation can then be inverted to retrieve the local intensity of the superimposed pump and Stokes beams:

$$\begin{pmatrix} I_p \\ I_S \\ U \end{pmatrix} = M^{-1} \begin{pmatrix} R \\ G \\ B \end{pmatrix},$$

where U represents an irrelevant output. Vertical and horizontal intensity profiles of both beams are then fitted with a Gaussian function that retrieves their position in the NF and FF. Thanks to four PID controllers implemented in LabView that act on piezoelectric actuators placed on two tip-tilt mirror mounts controlling transverse position and tilt of the Stokes beam, an active alignment of the Stokes onto the pump beam is eventually performed both in the NF and FF. Fig. 6b shows the effect of manual and automatic beam alignment on the retrieved centre frequency. Automatic beam alignment results in line centre fluctuations upon repeated measurements reduced to 65 kHz rms, at the level dictated by the statistical noise, as compared to fluctuations of more than 1 MHz with manual alignment.

3. Conclusions

We have presented and discussed in detail a Coherent Raman spectrometer for optical metrology of Raman-active transitions and in particular of weak quadrupole transitions that are relevance for fundamental physics. It makes use for the first time of an optical frequency comb to achieve a repeatable and accurate frequency axis calibration. This approach is suitable to probe with near-infrared lasers fundamental transitions that could be hardly addressed with similar signal-to-noise ratios by absorption spectrometers operating in the mid-infrared. The choice of an SRS regime adds a very high spectral fidelity that makes it of interest also for highly accurate measurements of molecular lineshapes and thus for collisional studies. The metrological capabilities of the spectrometer was recently demonstrated by the measurement of the transition frequency of the Q(1) 1-0 line of H2 at 4155 cm^{-1} with an accuracy of few parts-per-billion ($1.0 \cdot 10\text{-}5$ cm^{-1}), corresponding

to an improvement by a factor of 10 and 2, respectively, of the current experimental and theoretical benchmarks. With minor technical changes, namely the replacement of the pump laser, it is susceptible to address a two decades-spanning frequency range, from 50 to 5000 cm^{-1}, that covers all fundamental rovibrational bands as well as purely rotational bands.

As it is a nonlinear spectrometer where the signal scales linearly with the laser intensity and the interaction length, one may easily anticipate a substantial boost of the performance by replacement of the multipass cell with a hollow-core photonic crystal fibre (HC-PCF). In a multipass cell an effective interaction length of few tens of meters comes along with a spot size diameter of about 300 μm. An HC-PCF, which can provide the same interaction length with a 10 times smaller spot-size, is able to increase the intensity, and thus the signal-to-noise ratio by a factor of 100. This will be highly suitable to perform measurements at very low pressures [52] or under dilution with suitable collisional perturbers (e.g. He, Ar)[66] to further reduce the uncertainty budget on the final transition frequencies. The fibre environment is also of extreme interest to enter collisional regimes dominated by wall collisions that can significantly simplify the regression to zero pressure of the measured line centre frequencies. The upgrade of the spectrometer in this fibre perspective is currently in progress.

Funding

This work has received co-funding from the Horizon Europe Framework Programme (HORIZON) under grant agreement No 101047137 - TROPHY.

Disclosure statement

The authors report there are no competing interests to declare.

REFERENCES

[1] G. L. Eesley, “Coherent raman spectroscopy,” *J Quant Spectrosc Radiat Transf*, vol. 22, no. 6, pp. 507–576, Dec. 1979, doi: 10.1016/0022-4073(79)90045-1.

[2] A. D. Devir, "The determination of absolute Raman cross sections by indirect measurement of stimulated Raman gain," *J Appl Phys*, vol. 49, no. 6, pp. 3110–3113, Jun. 1978, doi: 10.1063/1.325301.

[3] D. Hanna, D. Pointer, and D. Pratt, "Stimulated Raman scattering of picosecond light pulses in hydrogen, deuterium, and methane," *IEEE J Quantum Electron*, vol. 22, no. 2, pp. 332–336, Feb. 1986, doi: 10.1109/JQE.1986.1072945.

[4] A. Kazzaz, S. Ruschin, I. Shoshan, and G. Ravnitsky, "Stimulated Raman scattering in methane-experimental optimization and numerical model," *IEEE J Quantum Electron*, vol. 30, no. 12, pp. 3017–3024, 1994, doi: 10.1109/3.362703.

[5] W. Stricker, M. Woyde, R. Lückerath, and V. Bergmann, "Temperature Measurements in High Pressure Combustion," *Berichte der Bunsengesellschaft für physikalische Chemie*, vol. 97, no. 12, pp. 1608–1618, Dec. 1993, doi: 10.1002/bbpc.19930971217.

[6] M. Pealat, J. P. E. Taran, J. Taillet, M. Bacal, and A. M. Bruneteau, "Measurement of vibrational populations in low-pressure hydrogen plasma by coherent anti-Stokes Raman scattering," *J Appl Phys*, vol. 52, no. 4, pp. 2687–2691, Apr. 1981, doi: 10.1063/1.329075.

[7] D. Robert, J. Bonamy, J. P. Sala, G. Levi, and F. Marsault-Herail, "Temperature dependence of the vibrational phase relaxation in gases: Application to H_2-rare gas mixtures," *Chem Phys*, vol. 99, no. 2, pp. 303–315, Oct. 1985, doi: 10.1016/0301-0104(85)80127-0.

[8] D. Polli, V. Kumar, C. M. Valensise, M. Marangoni, and G. Cerullo, "Broadband Coherent Raman Scattering Microscopy," *Laser Photon Rev*, vol. 12, no. 9, p. 1800020, Sep. 2018, doi: 10.1002/lpor.201800020.

[9] G. J. Rosasco, A. D. May, W. S. Hurst, L. B. Petway, and K. C. Smyth, "Broadening and shifting of the Raman *Q* branch of HD," *J Chem Phys*, vol. 90, no. 4, pp. 2115–2124, Feb. 1989, doi: 10.1063/1.456005.

[10] L. A. Rahn and G. J. Rosasco, "Measurement of the density shift of the H_2 *Q* (0–5) transitions from 295 to 1000 K," *Phys Rev A (Coll Park)*, vol. 41, no. 7, pp. 3698–3706, Apr. 1990, doi: 10.1103/PhysRevA.41.3698.

[11] L. A. Rahn, R. L. Farrow, and G. J. Rosasco, "Measurement of the self-broadening of the H_2 *Q* (0–5) Raman transitions from 295 to 1000 K," *Phys Rev A (Coll Park)*, vol. 43, no. 11, pp. 6075–6088, Jun. 1991, doi: 10.1103/PhysRevA.43.6075.

[12] P. M. Sinclair, P. Duggan, M. le Flohic, J. W. Forsman, J. R. Drummond, and A. D. May, "Broadening and shifting of the Raman *Q* branch in pure D_2 and D_2–He mixtures, I: experimental results and comparison with theory," *Can J Phys*, vol. 72, no. 11–12, pp. 885–890, Nov. 1994, doi: 10.1139/p94-116.

[13] P. M. Sinclair, P. Duggan, J. W. Forsman, J. R. Drummond, and A. D. May, "Broadening and shifting of the Raman *Q* branch in D_2 and D_2–He mixtures, II: line shapes, fitting routines, and effects nonlinear in density," *Can J Phys*, vol. 72, no. 11–12, pp. 891–896, Nov. 1994, doi: 10.1139/p94-117.

[14] W. K. Bischel and M. J. Dyer, "Temperature dependence of the Raman linewidth and line shift for the Q(1) and Q(0) transitions in normal and para-H_2," *Phys Rev A (Coll Park)*, vol. 33, no. 5, pp. 3113–3123, May 1986, doi: 10.1103/PhysRevA.33.3113.

[15] J. Ph. Berger, R. Saint-Loup, H. Berger, J. Bonamy, and D. Robert, "Measurement of vibrational line profiles in H_2–rare-gas mixtures: Determination of the speed dependence of the line shift," *Phys Rev A (Coll Park)*, vol. 49, no. 5, pp. 3396–3406, May 1994, doi: 10.1103/PhysRevA.49.3396.

[16] P. M. Sinclair *et al.*, "Collisional broadening and shifting parameters of the Raman *Q* branch of H_2 perturbed by N_2 determined from speed-dependent line profiles at high temperatures," *Phys Rev A (Coll Park)*, vol. 54, no. 1, pp. 402–409, Jul. 1996, doi: 10.1103/PhysRevA.54.402.

[17] J. D. Kelley and S. L. Bragg, "Effect of collisions on line profiles in the vibrational spectrum of molecular hydrogen," *Phys Rev A (Coll Park)*, vol. 34, no. 4, pp. 3003–3014, Oct. 1986, doi: 10.1103/PhysRevA.34.3003.

[18] X. Michaut, R. Saint-Loup, H. Berger, M. L. Dubernet, P. Joubert, and J. Bonamy, "Investigations of pure rotational transitions of H_2 self-perturbed and perturbed by He. I. Measurement, modeling, and quantum calculations," *J Chem Phys*, vol. 109, no. 3, pp. 951–961, Jul. 1998, doi: 10.1063/1.476638.

[19] M. P. le Flohic, P. Duggan, P. M. Sinclair, J. R. Drummond, and A. D. May, "Collisional broadening and shifting of the pure rotational Raman lines S_0 (J=0–4) of H_2 at room temperature," *Can J Phys*, vol. 72, no. 5–6, pp. 186–192, May 1994, doi: 10.1139/p94-029.

[20] R. L. Farrow and G. O. Sitz, "Coherent anti-Stokes Raman spectroscopy investigation of the anisotropic vibrational transitions of hydrogen," *Journal of the Optical Society of America B*, vol. 6, no. 5, p. 865, May 1989, doi: 10.1364/JOSAB.6.000865.

[21] P. M. Sinclair, P. Duggan, J. R. Drummond, and A. D. May, "Broadening and shifting of the depolarized component of the Raman *Q* branch in D_2 at room temperature," *Can J Phys*, vol. 73, no. 7–8, pp. 530–536, Jul. 1995, doi: 10.1139/p95-077.

[22] C. Schwartz and R. J. le Roy, "Nonadiabatic eigenvalues and adiabatic matrix elements for all isotopes of diatomic hydrogen," *J Mol Spectrosc*, vol. 121, no. 2, pp. 420–439, Feb. 1987, doi: 10.1016/0022-2852(87)90059-2.

[23] D. A. Shapiro, R. Ciurylo, R. Jaworski, and A. D. May, "Modeling the spectral line shapes with speed-dependent broadening and Dicke narrowing," *Can J Phys*, vol. 79, no. 10, pp. 1209–1222, Oct. 2001, doi: 10.1139/p01-080.

[24] J. Komasa, K. Piszczatowski, G. Łach, M. Przybytek, B. Jeziorski, and K. Pachucki, "Quantum Electrodynamics Effects in Rovibrational Spectra of Molecular Hydrogen," *J Chem Theory Comput*, vol. 7, no. 10, pp. 3105–3115, Oct. 2011, doi: 10.1021/ct200438t.

[25] E. J. Salumbides *et al.*, "Improved Laboratory Values of the H_2 Lyman and Werner Lines for Constraining Time Variation of the Proton-to-Electron Mass Ratio," *Phys Rev Lett*, vol. 101, no. 22, p. 223001, Nov. 2008, doi: 10.1103/PhysRevLett.101.223001.

[26] E. J. Salumbides, J. C. J. Koelemeij, J. Komasa, K. Pachucki, K. S. E. Eikema, and W. Ubachs, "Bounds on fifth forces from precision measurements on molecules," *Physical Review D*, vol. 87, no. 11, p. 112008, Jun. 2013, doi: 10.1103/PhysRevD.87.112008.

[27] E. J. Salumbides, A. N. Schellekens, B. Gato-Rivera, and W. Ubachs, "Constraints on extra dimensions from precision molecular spectroscopy," *New J Phys*, vol. 17, no. 3, p. 033015, Mar. 2015, doi: 10.1088/1367-2630/17/3/033015.

[28] W. Ubachs, J. C. J. Koelemeij, K. S. E. Eikema, and E. J. Salumbides, "Physics beyond the Standard Model from hydrogen spectroscopy," *J Mol Spectrosc*, vol. 320, pp. 1–12, Feb. 2016, doi: 10.1016/j.jms.2015.12.003.

[29] J. Komasa, M. Puchalski, P. Czachorowski, G. Łach, and K. Pachucki, "Rovibrational energy levels of the hydrogen molecule through nonadiabatic perturbation theory," *Phys Rev A (Coll Park)*, vol. 100, no. 3, p. 032519, Sep. 2019, doi: 10.1103/PhysRevA.100.032519.

[30] M. L. Niu, E. J. Salumbides, G. D. Dickenson, K. S. E. Eikema, and W. Ubachs, "Precision spectroscopy of the X1Σg+, v=0→1(J=0–2) rovibrational splittings in H_2,

HD and D_2," *J Mol Spectrosc*, vol. 300, pp. 44–54, Jun. 2014, doi: 10.1016/j.jms.2014.03.011.

[31] S. L. Bragg, W. H. Smith, and J. W. Brault, "Line positions and strengths in the H_2 quadrupole spectrum," *Astrophys J*, vol. 263, p. 999, Dec. 1982, doi: 10.1086/160568.

[32] A. Fast and S. A. Meek, "Precise measurement of the D_2 $S_1(0)$ vibrational transition frequency," *Mol Phys*, Nov. 2021, doi: 10.1080/00268976.2021.1999520.

[33] D. Romanini, I. Ventrillard, G. Méjean, J. Morville, and E. Kerstel, "Introduction to Cavity Enhanced Absorption Spectroscopy," 2014, pp. 1–60. doi: 10.1007/978-3-642-40003-2_1.

[34] S. Kassi and A. Campargue, "Electric quadrupole and dipole transitions of the first overtone band of HD by CRDS between 1.45 and 1.33 μm," *J Mol Spectrosc*, vol. 267, no. 1–2, pp. 36–42, May 2011, doi: 10.1016/j.jms.2011.02.001.

[35] S. Kassi, A. Campargue, K. Pachucki, and J. Komasa, "The absorption spectrum of D_2 : Ultrasensitive cavity ring down spectroscopy of the (2–0) band near 1.7 μm and accurate *ab initio* line list up to 24000 cm^{-1}," *J Chem Phys*, vol. 136, no. 18, p. 184309, May 2012, doi: 10.1063/1.4707708.

[36] A. Campargue, S. Kassi, K. Pachucki, and J. Komasa, "The absorption spectrum of H_2: CRDS measurements of the (2-0) band, review of the literature data and accurate ab initio line list up to 35000 cm^{-1}," *Phys. Chem. Chem. Phys.*, vol. 14, no. 2, pp. 802–815, 2012, doi: 10.1039/C1CP22912E.

[37] D. Mondelain, S. Kassi, T. Sala, D. Romanini, D. Gatti, and A. Campargue, "Sub-MHz accuracy measurement of the S(2) 2–0 transition frequency of D_2 by Comb-Assisted Cavity Ring Down spectroscopy," *J Mol Spectrosc*, vol. 326, pp. 5–8, Aug. 2016, doi: 10.1016/j.jms.2016.02.008.

[38] E. Fasci, A. Castrillo, H. Dinesan, S. Gravina, L. Moretti, and L. Gianfrani, "Precision spectroscopy of HD at 1.38μm," *Phys Rev A (Coll Park)*, vol. 98, no. 2, p. 022516, Aug. 2018, doi: 10.1103/PhysRevA.98.022516.

[39] P. Wcisło *et al.*, "Accurate deuterium spectroscopy for fundamental studies," *J Quant Spectrosc Radiat Transf*, vol. 213, pp. 41–51, Jul. 2018, doi: 10.1016/j.jqsrt.2018.04.011.

[40] D. Mondelain, S. Kassi, and A. Campargue, "Transition frequencies in the (2-0) band of D_2 with MHz accuracy," *J Quant Spectrosc Radiat Transf*, vol. 253, p. 107020, Sep. 2020, doi: 10.1016/j.jqsrt.2020.107020.

[41] S. Wójtewicz *et al.*, "Accurate deuterium spectroscopy and comparison with *ab initio* calculations," *Phys Rev A (Coll Park)*, vol. 101, no. 5, p. 052504, May 2020, doi: 10.1103/PhysRevA.101.052504.

[42] M. Zaborowski *et al.*, "Ultrahigh finesse cavity-enhanced spectroscopy for accurate tests of quantum electrodynamics for molecules," *Opt Lett*, vol. 45, no. 7, p. 1603, Apr. 2020, doi: 10.1364/OL.389268.

[43] P. Wcisło *et al.*, "The implementation of non-Voigt line profiles in the HITRAN database: H_2 case study," *J Quant Spectrosc Radiat Transf*, vol. 177, pp. 75–91, Jul. 2016, doi: 10.1016/j.jqsrt.2016.01.024.

[44] P. Wcisło, I. E. Gordon, C.-F. Cheng, S.-M. Hu, and R. Ciuryło, "Collision-induced line-shape effects limiting the accuracy in Doppler-limited spectroscopy of H_2," *Phys Rev A (Coll Park)*, vol. 93, no. 2, p. 022501, Feb. 2016, doi: 10.1103/PhysRevA.93.022501.

[45] M. Konefał, M. Słowiński, M. Zaborowski, R. Ciuryło, D. Lisak, and P. Wcisło, "Analytical-function correction to the Hartmann–Tran profile for more reliable representation of the Dicke-narrowed molecular spectra," *J Quant Spectrosc Radiat Transf*, vol. 242, p. 106784, Feb. 2020, doi: 10.1016/j.jqsrt.2019.106784.

[46] J. Tennyson *et al.*, "Recommended isolated-line profile for representing high-resolution spectroscopic transitions (IUPAC Technical Report)," *Pure and Applied Chemistry*, vol. 86, no. 12, pp. 1931–1943, Dec. 2014, doi: 10.1515/pac-2014-0208.

[47] M. Słowiński *et al.*, "H_2-He collisions: *Ab initio* theory meets cavity-enhanced spectra," *Phys Rev A (Coll Park)*, vol. 101, no. 5, p. 052705, May 2020, doi: 10.1103/PhysRevA.101.052705.

[48] R. Z. Martínez, D. Bermejo, F. Thibault, and P. Wcisło, "Testing the ab initio quantum-scattering calculations for the D_2-He benchmark system with stimulated Raman spectroscopy," *Journal of Raman Spectroscopy*, vol. 49, no. 8, pp. 1339–1349, Aug. 2018, doi: 10.1002/jrs.5391.

[49] A. Fast and S. A. Meek, "Sub-ppb Measurement of a Fundamental Band Rovibrational Transition in HD," *Phys Rev Lett*, vol. 125, no. 2, p. 023001, Jul. 2020, doi: 10.1103/PhysRevLett.125.023001.

[50] F. M. J. Cozijn, P. Dupré, E. J. Salumbides, K. S. E. Eikema, and W. Ubachs, "Sub-Doppler Frequency Metrology in HD for Tests of Fundamental Physics," *Phys Rev Lett*, vol. 120, no. 15, p. 153002, Apr. 2018, doi: 10.1103/PhysRevLett.120.153002.

[51] L.-G. Tao *et al.*, "Toward a Determination of the Proton-Electron Mass Ratio from the Lamb-Dip Measurement of HD," *Phys Rev Lett*, vol. 120, no. 15, p. 153001, Apr. 2018, doi: 10.1103/PhysRevLett.120.153001.

[52] S. Kassi, C. Lauzin, J. Chaillot, and A. Campargue, "The (2–0) *R* (0) and *R* (1) transition frequencies of HD determined to a 10^{-10} relative accuracy by Doppler spectroscopy at 80 K," *Physical Chemistry Chemical Physics*, vol. 24, no. 38, pp. 23164–23172, 2022, doi: 10.1039/D2CP02151J.

[53] A. Castrillo, E. Fasci, and L. Gianfrani, "Doppler-limited precision spectroscopy of HD at 1.4μm: An improved determination of the R(1) centre frequency," *Phys Rev A (Coll Park)*, vol. 103, no. 2, p. 022828, Feb. 2021, doi: 10.1103/PhysRevA.103.022828.

[54] F. M. J. Cozijn, M. L. Diouf, V. Hermann, E. J. Salumbides, M. Schlösser, and W. Ubachs, "Rotational level spacings in HD from vibrational saturation spectroscopy," *Phys Rev A (Coll Park)*, vol. 105, no. 6, p. 062823, Jun. 2022, doi: 10.1103/PhysRevA.105.062823.

[55] M. L. Diouf, F. M. J. Cozijn, B. Darquié, E. J. Salumbides, and W. Ubachs, "Lamb-dips and Lamb-peaks in the saturation spectrum of HD," *Opt Lett*, vol. 44, no. 19, p. 4733, Oct. 2019, doi: 10.1364/OL.44.004733.

[56] T.-P. Hua, Y. R. Sun, and S.-M. Hu, "Dispersion-like lineshape observed in cavity-enhanced saturation spectroscopy of HD at 1.4μm," *Opt Lett*, vol. 45, no. 17, p. 4863, Sep. 2020, doi: 10.1364/OL.401879.

[57] Y.-N. Lv *et al.*, "Nonlinear Fano resonance without a continuum," Mar. 2022.

[58] K.-F. Lai *et al.*, "Precision measurement of the fundamental vibrational frequencies of tritium-bearing hydrogen molecules: T_2, DT, HT," *Physical Chemistry Chemical Physics*, vol. 22, no. 16, pp. 8973–8987, 2020, doi: 10.1039/D0CP00596G.

[59] F. Thibault, R. Z. Martínez, D. Bermejo, and P. Wcisło, "Line-shape parameters for the first rotational lines of HD in He," *Mol Astrophys*, vol. 19, p. 100063, Jun. 2020, doi: 10.1016/j.molap.2020.100063.

[60] L. A. Rahn and R. E. Palmer, "Studies of nitrogen self-broadening at high temperature with inverse Raman spectroscopy," *Journal of the Optical Society of America B*, vol. 3, no. 9, p. 1164, Sep. 1986, doi: 10.1364/JOSAB.3.001164.

[61] A. Owyoung, "Coherent Raman gain spectroscopy using CW laser sources," *IEEE J Quantum Electron*, vol. 14, no. 3, pp. 192–203, Mar. 1978, doi: 10.1109/JQE.1978.1069760.

[62] G. J. Rosasco and W. S. Hurst, "Phase-modulated stimulated Raman spectroscopy," *Journal of the Optical Society of America B*, vol. 2, no. 9, p. 1485, Sep. 1985, doi: 10.1364/JOSAB.2.001485.

[63] J. W. Forsman, P. M. Sinclair, P. Duggan, J. R. Drummond, and A. D. May, "A high-resolution Raman gain spectrometer for spectral lineshape studies," *Can J Phys*, vol. 69, no. 5, pp. 558–563, May 1991, doi: 10.1139/p91-092.

[64] M. Lamperti *et al.*, "Stimulated-Raman-Scattering Metrology," Jul. 2022, https://arxiv.org/abs/2207.03998.

[65] J. B. McManus, P. L. Kebabian, and M. S. Zahniser, "Astigmatic mirror multipass absorption cells for long-path-length spectroscopy," *Appl Opt*, vol. 34, no. 18, p. 3336, Jun. 1995, doi: 10.1364/AO.34.003336.

[66] E. A. Serov *et al.*, "CO-Ar collisions: ab initio model matches experimental spectra at a sub percent level over a wide pressure range," *J Quant Spectrosc Radiat Transf*, vol. 272, p. 107807, Sep. 2021, doi: 10.1016/j.jqsrt.2021.107807.

FIGURE 1. Optical layout of SRS the spectrometer. Coloured boxes encase the parts of the setup described in detail in the sections of the main text. AOM: acousto-optic modulator; D: (beam) dump; EOM: electro-optical modulator; RF: radiofrequency signal; PZT: piezoelectric actuator; BC: beam combiner; DM: dichroic mirror; HPF: high-pass filter; BS: beam splitter; NDF: neutral density filter; SRL: stimulated Raman loss signal; DAQ: digital acquisition board; BD: balanced detector; LPF: low-pass filter; BPF: band-pass filter; PPLN: periodically-poled lithium niobate crystal; PPSLT: periodically-poled stoichiometric lithium tantalate crystal; PFD: phase-frequency detector; PID: proportional-integral-derivative controller.

FIGURE 2. Beat notes electrical spectra. Spectra are normalized to bring both peaks at the 0 dB level for easier visual comparison.

FIGURE 3. Noise performance. a) Comparison of the detection noise with the shot noise level. From top to bottom in the legend: lock-in noise floor, detector noise, noise spectrum of the pump laser impinging on the detector, shot noise level calculated for the pump power impinging on the detector (350 μW), calculated detector noise for a shot-noise limited beam impinging on the detector. b) Normalized SRL spectra of the Q(1) 1-0 line of H_2 measured at different pressures. The first number in the legend represents the measurement pressure in bar, the second one is the SNR of the spectrum.

FIGURE 4. Active stabilization of laser power. Power fluctuations of the Stokes beam relative to the power at t = 0 when the active stabilization is inactive (red trace) or active (blue trace), in the case fixed Stokes laser frequency (a) and b) scanning Stokes frequency (b), over about 10 GHz at a rate of 1 Hz.

FIGURE 5. Stokes frequency calibration. a) Time-trace of the beat note frequency $f_{bn,s}$ between Stokes laser and comb during a spectral acquisition, as measured by the acquisition card. b) Unwrapped $f_{bn,s}$ used to calibrate the spectral frequency axis. c) SRL signal synchronously

acquired by the card.

FIGURE 6. Active beam alignment. a) Schematic diagram of the active beam alignment system; NF: near field; FF: far field. b) Fluctuations of the line centre frequency over different measurements with the gas kept at constant thermodynamic conditions and the Stokes beam misaligned and realigned onto the pump beam before each measurement. Red dots (measurements 1-8) represent measurements where the alignment is manual, while blue dots (9-15) represent measurements under active beam alignment. Each dot corresponds to an averaged spectrum acquired over 5 min, while error bars are the standard deviation of the mean. The vertical scale is relative to the mean line centre frequency retrieved with active stabilization.

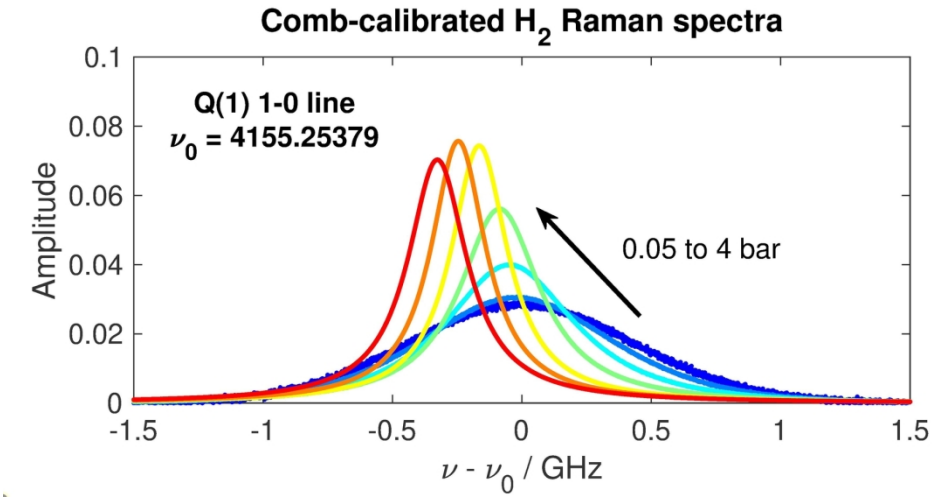

Stimulated Raman spectra of the Q(1) 1-0 transition of H_2 measured at different pressures. The curves are normalized to unitary area, and v_0 represents the extrapolated zero-pressure transition frequency.

162x81mm (300 x 300 DPI)

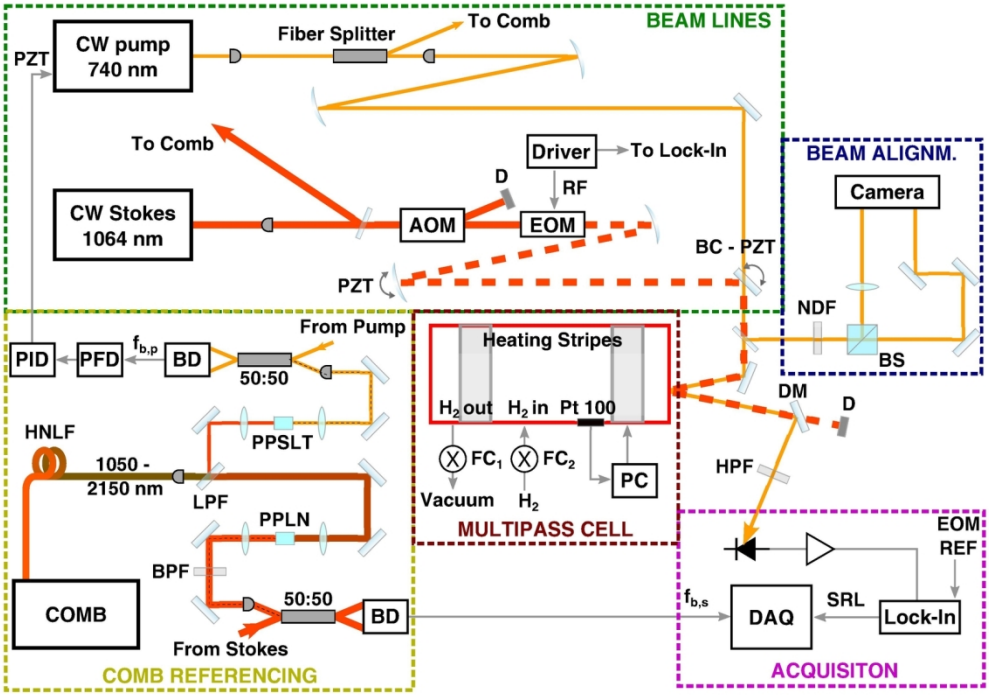

Optical layout of SRS the spectrometer. Coloured boxes encase the parts of the setup described in detail in the sections of the main text. AOM: acousto-optic modulator; D: (beam) dump; EOM: electro-optical modulator; RF: radiofrequency signal; PZT: piezoelectric actuator; BC: beam combiner; DM: dichroic mirror; HPF: high-pass filter; BS: beam splitter; NDF: neutral density filter; SRL: stimulated Raman loss signal; DAQ: digital acquisition board; BD: balanced detector; LPF: low-pass filter; BPF: band-pass filter; PPLN: periodically-poled lithium niobate crystal; PPSLT: periodically-poled stoichiometric lithium tantalate crystal; PFD: phase-frequency detector; PID: proportional-integral-derivative controller.

147x104mm (300 x 300 DPI)

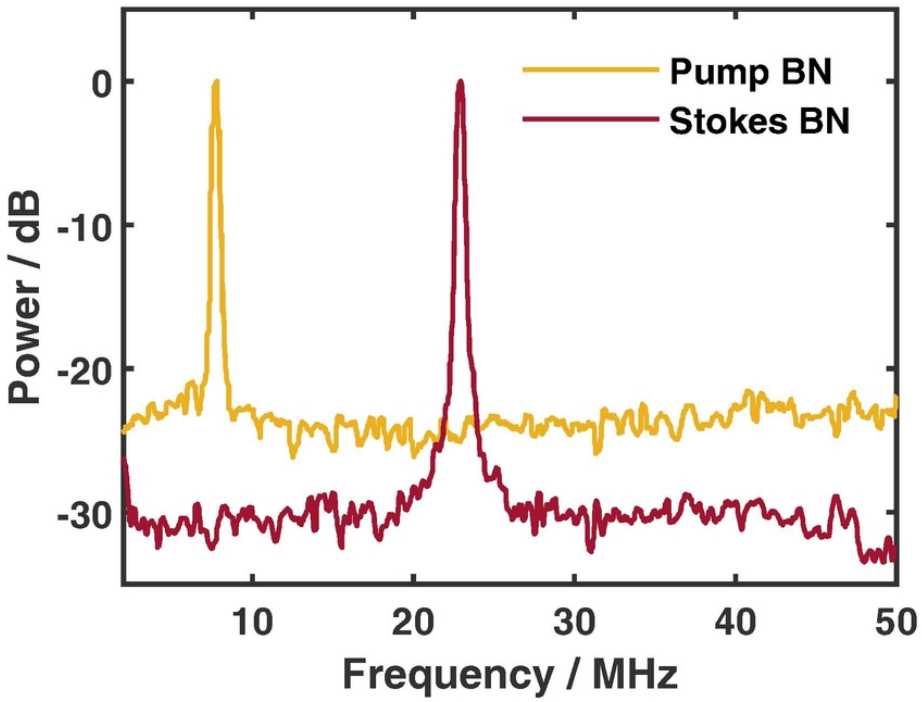

Beat notes electrical spectra. Spectra are normalized to bring both peaks at the 0 dB level for easier visual comparison.

77x58mm (300 x 300 DPI)

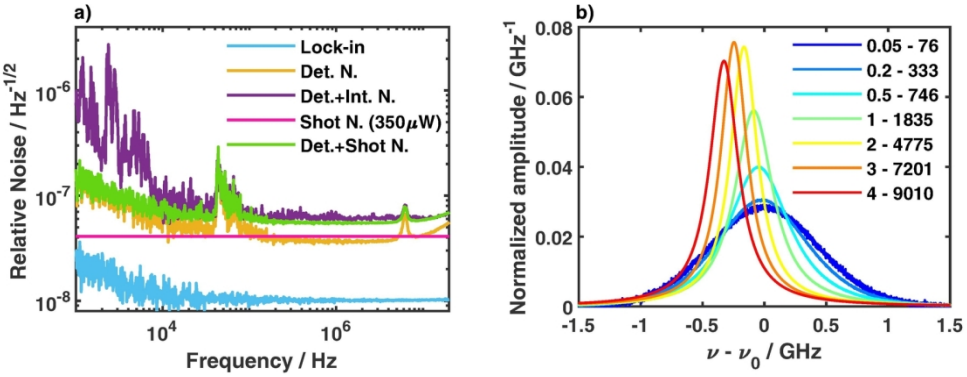

Noise performance. a) Comparison of the detection noise with the shot noise level. From top to bottom in the legend: lock-in noise floor, detector noise, noise spectrum of the pump laser impinging on the detector, shot noise level calculated for the pump power impinging on the detector (350 μW), calculated detector noise for a shot-noise limited beam impinging on the detector. b) Normalized SRL spectra of the Q(1) 1-0 line of H2 measured at different pressures. The first number in the legend represents the measurement pressure in bar, the second one is the SNR of the spectrum.

155x58mm (300 x 300 DPI)

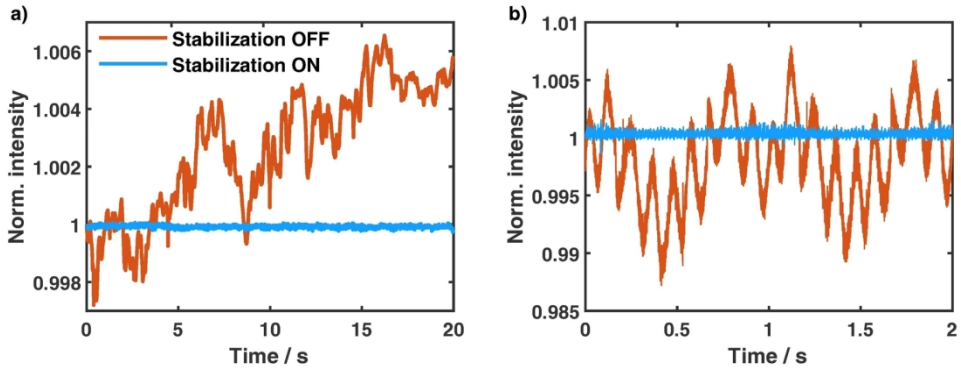

Active stabilization of laser power. Power fluctuations of the Stokes beam relative to the power at t = 0 when the active stabilization is inactive (red trace) or active (blue trace), in the case fixed Stokes laser frequency (a) and b) scanning Stokes frequency (b), over about 10 GHz at a rate of 1 Hz.

155x58mm (300 x 300 DPI)

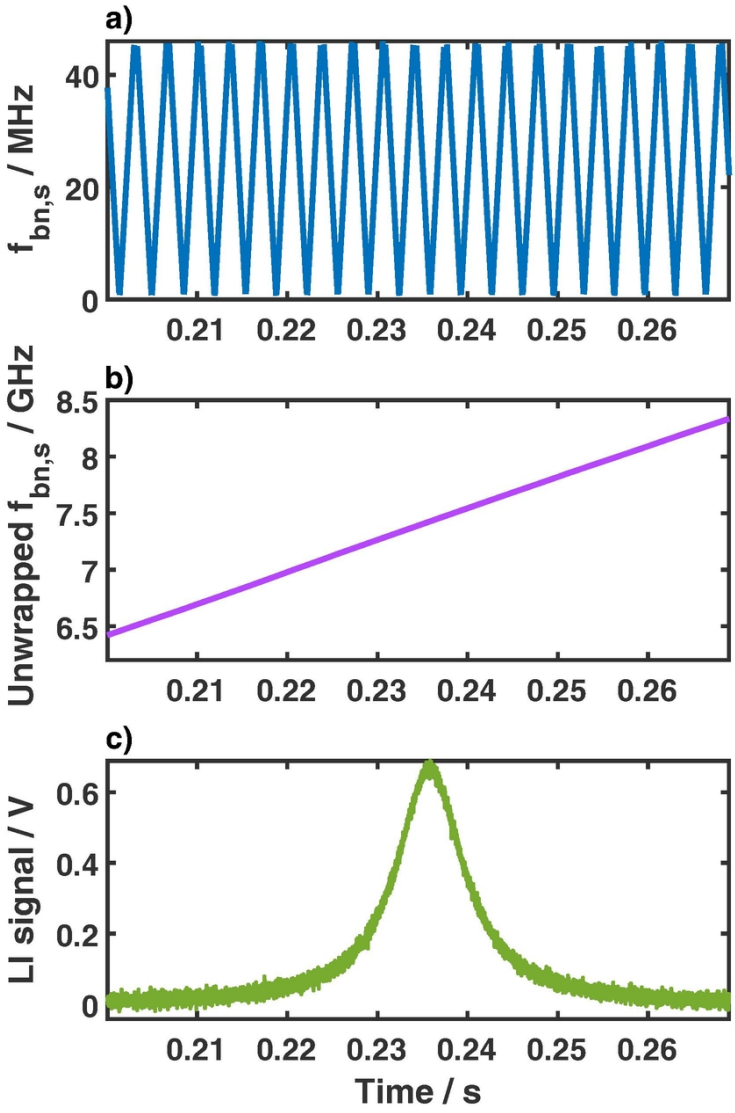

Stokes frequency calibration. a) Time-trace of the beat note frequency f_(bn,s) between Stokes laser and comb during a spectral acquisition, as measured by the acquisition card. b) Unwrapped f_(bn,s) used to calibrate the spectral frequency axis. c) SRL signal synchronously acquired by the card.

77x115mm (300 x 300 DPI)

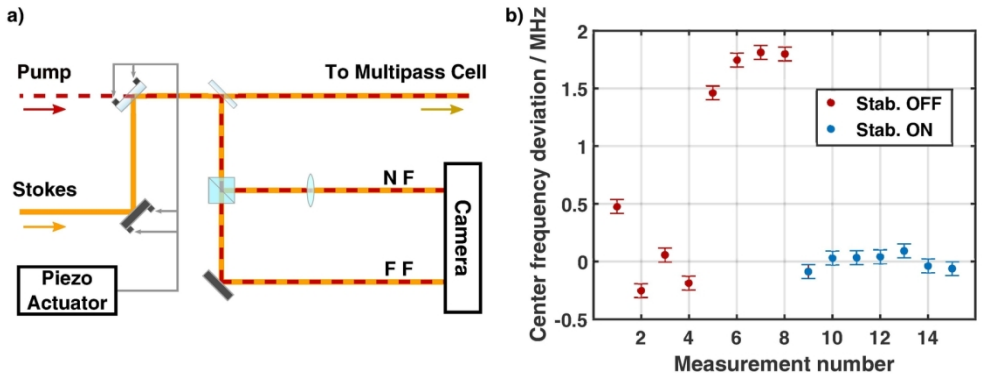

a) Schematic diagram of the active beam alignment system; NF: near field; FF: far field. b) Fluctuations of the line centre frequency over different measurements with the gas kept at constant thermodynamic conditions and the Stokes beam misaligned and realigned onto the pump beam before each measurement. Red dots (measurements 1-8) represent measurements where the alignment is manual, while blue dots (9-15) represent measurements under active beam alignment. Each dot corresponds to an averaged spectrum acquired over 5 min, while error bars are the standard deviation of the mean. The vertical scale is relative to the mean line centre frequency retrieved with active stabilization.

155x58mm (300 x 300 DPI)